PCCP

Implications of the Fractional Charge of Hydroxide at the Electrochemical Interface

Journal:	*Physical Chemistry Chemical Physics*
Manuscript ID	CP-ART-11-2019-005952.R3
Article Type:	Paper
Date Submitted by the Author:	07-Feb-2020

Complete List of Authors:	Gauthier, Joseph; Stanford University, Chemical Engineering Chen, Leanne; University of Guelph, Chemistry Bajdich, Michal; e. SUNCAT Center for Interface Science and Catalysis, SLAC National Accelerator Laboratory, Menlo Park, California 94025, United States, SUNCAT; Stanford University, SLAC STANFORD Chan, Karen; Technical University of Denmark,

PCCP

ARTICLE TYPE

Cite this: DOI: 00.0000/xxxxxxxxxx

Implications of the Fractional Charge of Hydroxide at the Electrochemical Interface†

Joseph A. Gauthier,[a,b] Leanne D. Chen,[a‡] Michal Bajdich,[b] and Karen Chan*[c]

Received Date
Accepted Date

DOI: 00.0000/xxxxxxxxxx

Rational design of materials that efficiently convert electrical energy into chemical bonds will ultimately depend on a thorough understanding of the electrochemical interface at the atomic level. Towards this goal, the use of density functional theory (DFT) at the generalized gradient approximation (GGA) level has been applied widely in the past 15 years. In the calculation of electrochemical reaction energetics using GGA-DFT, it is frequently implicitly assumed that ions in the Helmholtz plane have unit charge. However, the ion charge is observed to be fractional near the interface through both a capacitor model and through Bader charge partitioning. In this work, we show that this spurious charge transfer can be effectively mitigated by continuum charging of the electrolyte. We then show that, similar to hydronium, the observed fractional charge of hydroxide is not due to a GGA level self-interaction error, as the partial charge is observed even when using hybrid level exchange-correlation functionals.

1 Introduction

The electrochemical conversion of chemicals into value added-commodity products has been a growing interest to the scientific community in the past several decades, owing largely to the rapidly decreasing cost of renewable electricity from solar photovoltaics.[1,2] The rapid decrease in the cost of electricity allows processes such as the reduction of CO_2 and N_2 closer to be increasingly commercially viable despite significant limitations by poor catalytic activities of current catalysts[3–8] In particular, CO_2 and N_2 reduction catalysts are both limited by activity and selectivity. Ultimately, the rational design of catalysts for these and other related processes will rely on a detailed, atomic-scale understanding of the electrochemical interface.[9–12] Computational efforts in this space are dominated by density functional theory (DFT) methods at the generalized gradient approximation (GGA) level, since these offer a good balance between cost and accuracy.[13–15] However, GGA-DFT methods have long been known to suffer from a self-interaction error.[16–20] This error has several manifestations,[21] including poor prediction of band gaps of semiconducting materials,barriers of chemical reactions, energies of dissociating molecular ions, and charge transfer excitation energies. The same manifestation of the self-interaction error associated with poor band gap prediction can lead to spurious charge transfer (SCT) between the electrolyte and metal slab in electrochemical systems if the electrolyte band gap does not properly straddle the metal Fermi level.[16,22]

In a recent study,[23] we showed using higher level hybrid DFT methods that the observed partial charge on hydronium is not caused by these delocalization errors in GGA-DFT. Rather, it is a physical electron charge density overlap between the ion and the nearby metal surface. Peterson et al. recently confirmed[24] the finding of non-unity charge of hydronium near both platinum and gold close-packed surfaces. The extension of this argument to the case of anions such as hydroxide is technically complicated by the aforementioned issues of SCT, where the highest occupied molecular orbital (HOMO) of the hydroxide ion often aligns with the metal Fermi level for metals with a relatively large work function such as Pt. Andreussi et al. recently showed that halogen anions ~10 Å from a metal surface can be effectively modeled by embedding them in a dielectric medium.[25] In this work, we show that the challenge of SCT can be effectively mitigated by the placement of an excess surface charge density, with counter charges described by, e.g., the linearized Poisson-Boltzmann equation, in addition to the dielectric embedding. The excess surface charge shifts the metal Fermi level relative to the ion HOMO. This approach is similar to the one taken by Rossmeisl et al.,[22] where a homogeneous background charge with no dielectric continuum was used to simulate the counter charge. When the electrolyte

[a] SUNCAT Center for Interface Science and Catalysis, Department of Chemical Engineering, Stanford University, Stanford, California 94305, United States
[b] SUNCAT Center for Interface Science and Catalysis, SLAC National Accelerator Laboratory, 2575 Sand Hill Road, Menlo Park, California 94025, United States
[c] Department of Physics, Technical University of Denmark, DK-2800, Kgs. Lyngby, Denmark; E-mail: kchan@fysik.dtu.dk

† Electronic Supplementary Information (ESI) available: [ESI includes further details regarding the charge overlap analysis in the case of hydroxide, as well as geometry and input files necessary to reproduce all figures included in the main text]. See DOI: 10.1039/cXCP00000x/

‡ Present address: Department of Chemistry, University of Guelph, Guelph, ON N1G 2W1, Canada

bands properly straddle the metal Fermi level, i.e. the Fermi level lies within the electrolyte bandgap without any alignment with either the HOMO or the lowest unoccupied molecular orbital (LUMO) bands, we show that the partial charge observed on hydroxide is also not caused by delocalization errors. The fractional charge of hydroxide has implications for kinetic studies of alkaline reactions, where hydroxide at the interface plays a critical role.

2 Theoretical methods and models

This work uses the Vienna Ab initio Simulation Package[26–28] in conjunction with the added functionality of implicit solvation provided by VASPsol.[29,30] Core electrons are described as projector augmented wave pseudopotentials,[31] while valence electrons are expanded as plane-waves up to a kinetic energy cutoff of 400 eV. Electron exchange and correlation interactions are accounted for using the PBE functional[32] at the GGA level and with the HSE06[33] functional for hybrid-level calculations. Higher proportions of exact exchange were not considered due to the difficulty of achieving a self-consistent density for these metallic systems. When optimizing bulk platinum to determine the appropriate lattice constant, the Brillouin zone is sampled with a $12\times 12 \times 12$ γ-centered Monkhorst-Pack[34] k-point mesh. The optimized lattice constant is determined to be 3.968 Å for PBE functional, which is very close to exprimental value of 3.912 Å.[35]

A 3×3 supercell of Pt (111) surface with a single bilayer of water is used as the model system. A slab thickness of 3 layers, with the bottom two layers being fixed at the bulk lattice constant value, is used to describe the electrode. A complete monolayer of hydrogen is placed on the surface to facilitate stabilization of the hydroxide ion. The geometries are optimized in the case of a hydronium and hydroxide in the water layer, separately; in both cases, the ions form hydrogen bonds with the surrounding water molecules. The forces are minimized until the maximum force on all unconstrained atoms is less than 0.03 eV Å^{-1}. The solvent bilayer is systematically moved away from the surface to probe the effect of distance from the surface on the calculated ion charge. For these calculations, single-point energy calculations are performed to prevent water reorganization from complicating the calculated electron distribution or density of states (DOS). The computational and structural data is also available online at Catalysis-hub.org.[36,37]

VASPsol treats the electrolyte at the electrochemical interface as a polarizable continuum, placing point counter-charges via the linearized Poisson-Boltzmann equation. A Debye screening length of 3 Å is chosen, which corresponds to a bulk electrolyte concentration of 1 Molar. As described in a recent work,[38] the non-electrostatic coefficient is set to zero to avoid numerical instabilities in the electrolyte region. Details regarding the implementation of VASPsol can be found in its documentation.[29,30]

Ionic charges are determined through the Bader charge partitioning scheme,[39–41] which is used to calculate the charge on each atom by subtracting the expected number of electrons on the neutral atom. Due to the ambiguity intrinsic to charge partitioning (i.e. shared electrons between covalently bonded atoms), when calculating the ionic charge, we sum the charge of every atom in the solvent layer.

3 Results and discussion

We begin by showing that the previously reported spurious charge transfer associated with DFT calculated band misalignment[21,22], exacerbated by solvated ions at the interface, can be mitigated through the use of continuum charging. This is similar to the homogeneously charged background approach previously used.[22] By charging the surface, the Fermi level can be shifted relative to the electrolyte HOMO sufficiently to avoid SCT. This charging method allows us to investigate the behavior of anions at the interface where previously SCT made this impractical, and find that the charge of hydroxide remains fractional when in close proximity to the surface. We then show that the fractional charge of ions near the charged electrochemical interface is not limited to GGA level delocalization errors by comparing to hybrid-level (HSE06[33,42]) calculations, which was recently shown to compare favorably to higher level wavefunction methods on transition metal systems.[43] Previous analysis of the hydronium ion rationalized the partial charge by the asymmetric overlap of electron charge density between the metal slab and the ion in solution. We show here that the non-unity charge on hydroxide is not caused by DFT delocalization errors, however additional considerations are also required in contrast to hydronium.

3.1 Avoiding spurious charge transfer with continuum charging

Recently, the well-known challenge of DFT systematically underpredicting band gaps[21] was shown to occasionally cause spurious charge transfer at the metal/electrolyte interface,[22] by either the HOMO or LUMO of the electrolyte not appropriately straddling the metal Fermi level. This challenge, commonly referred to as SCT, is in practice exacerbated by ions (especially anions[25]) at the electrochemical interface.

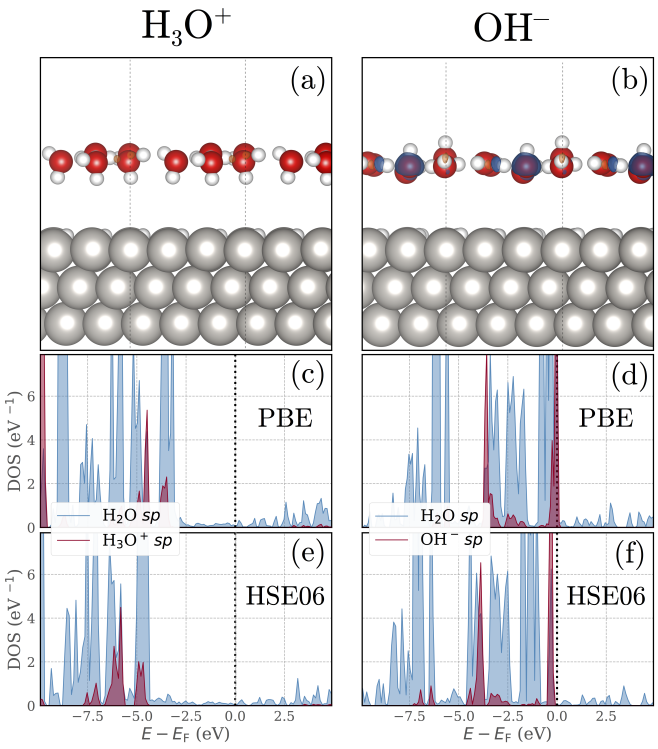

Fig. 1 Charge density difference between hybrid and GGA level DFT calculations corresponding to (a) a case with a hydronium ion near the surface, not showing SCT, and (b) a case with a hydroxide ion near the surface, showing SCT. The isosurface values of $\pm 2.5 \cdot 10^{-3}$ eÅ^{-3} corresponds to higher electron density (orange, more negatively charged) and lower electron density (blue, more positively charged). Illustrated here is the spurious transfer of charge from the electrolyte to the metal surface, totalling about 0.2 electrons. Panels (c) and (d) show the projected density of states (pDOS) at the GGA level for hydronium and hydroxide, respectively, where the incorrect extension of the hydroxide HOMO to above the Fermi level is clearly seen in panel (d). Finally, panels (e) and (f) show the pDOS at the hybrid level for hydronium and hydroxide, respectively; with the hybrid functional, the HOMO of hydroxide is shifted to be correctly below the Fermi level.

The lower edge of the LUMO for cations tends to be positioned below the Fermi level, while the upper edge of the HOMO for anions often extends above the Fermi level. This band misalignment results in the spurious transfer of electrons from the metal to the ion in the former case, and from ion to metal in the latter case. To illustrate this effect of GGA-DFT overdelocalizing electrons compared to hybrid-DFT, we calculate a charge density difference ρ_{diff} as:

$$\rho_{\text{diff}} = \rho_{\text{GGA}} - \rho_{\text{HSE06}}. \quad (1)$$

Here ρ_{diff} is the charge density difference, ρ_{GGA} is the charge density calculated at the GGA level using PBE as the exchange-correlation functional, and ρ_{HSE06} is the charge density calculated using a single-point calculation on the GGA level geometry. Figure 1, panels (a) and (b), show this charge density difference for a case not showing SCT (hydronium) and a case showing SCT (hydroxide), respectively. The geometries shown correspond to the explicit solvent bilayer shifted about 2 Å from the equilibrium position, where the misalignment becomes more pronounced, to more clearly demonstrate SCT.

Figure 1 (c) and (e) shows the projected density of states (pDOS) of the electrochemical interface with a hydronium ion in the outer Helmholtz plane at the GGA and hybrid level, respectively. In both cases, the electrolyte has no states at the Fermi level, indicating that the system is not exhibiting SCT. In these systems, the ionic charge was determined to be $1.0e$ at both the GGA and hybrid level. The charge here is not fractional since the bilayer has been shifted away from the surface. This offset effectively removes the electron density overlap effect previously reported for acidic conditions.[23].

A similar analysis is shown for the case of a hydroxide ion in the outer Helmholtz plane in Figure 1 (d) and (f), at the GGA and hybrid levels, respectively. Here the hydroxide ion shows a clear case of SCT at the GGA level, with the hydroxide HOMO states spilling over the metal Fermi level. This results in spurious charge transfer from the electrolyte to the metal, causing the predicted ionic charge to differ: a charge of $0.81e$ at the GGA level, and a charge of $1.0e$ at the hybrid level.

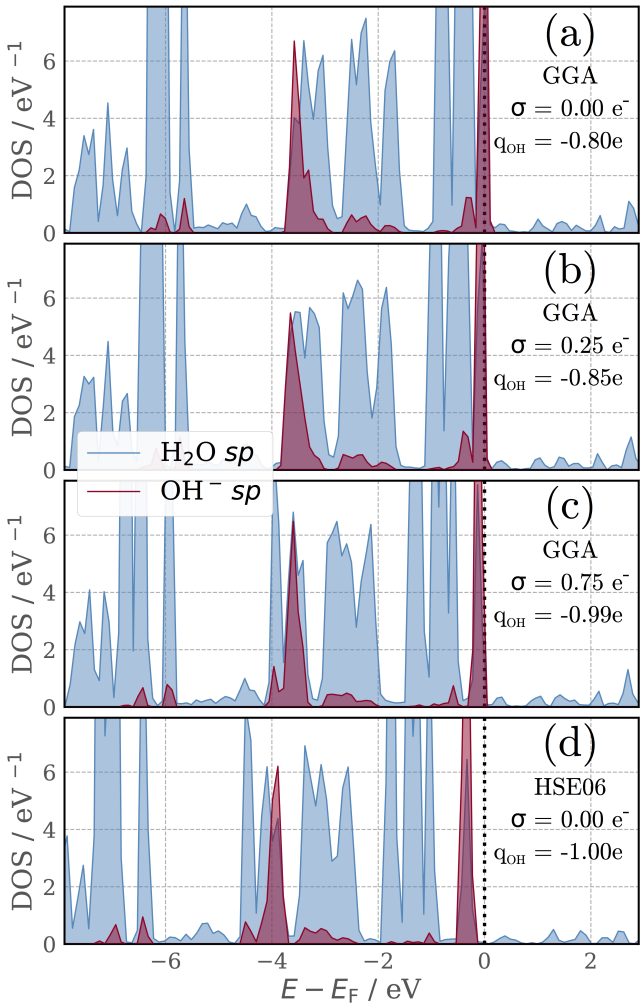

Fig. 2 Illustration of the mitigation of SCT by continuum charging. By increasing the surface charge density, the HOMO energies of both the ion and the solvent are lowered relative to the metal Fermi level. Panels (a), (b), and (c) show the pDOS of the electrolyte at the GGA level for an increasing surface charge density. Panel (d) shows the pDOS at the hybrid level.

Similar to what was shown in Ref. 22, SCT can be mitigated by increasing or decreasing the electron density on the metal surface. We demonstrate this here by charging the surface, with the placement of counter-charges determined by solving the linearized Poisson-Boltzmann equation as implemented in VASPsol, thereby retaining overall charge neutrality of the system. In Figure 2, we plot the pDOS of the water and hydroxide ion at the GGA level for three different surface charges σ, and at the hybrid level in a simulation without excess charging of the surface. As the surface charge density is systematically increased, the hydroxide HOMO is shifted negatively, until there is no spillover to above the Fermi level at a charge of $\sigma = 0.75$ excess electrons, i.e. the integral of hydroxide pDOS states above the Fermi level is equal to zero.

3.2 Implications of the fractional charge of hydroxide

With the ability to mitigate SCT by charging the surface established, we now turn our attention to rationalizing the observed fractional charge of the hydroxide ion near the metal surface. We follow a similar approach to our previous work,[23] and calculate the charge on different parts of the system as the ion is systematically moved from its equilibrium position at the interface. Single point calculations are performed at each position to prevent water structure reorientation from conflating the resulting charge calculation, illustrated in Figure 3. Additional charging cases, including cases without the inclusion of a dielectric continuum to stabilize the ions far from the surface, can be found in SI Note 3, Figure S3. In particular, without the stabilizing effect of the dielectric, the charge of both hydronium and hydroxide decays substantially far from the surface, as was found by Nattino and coworkers.[25]

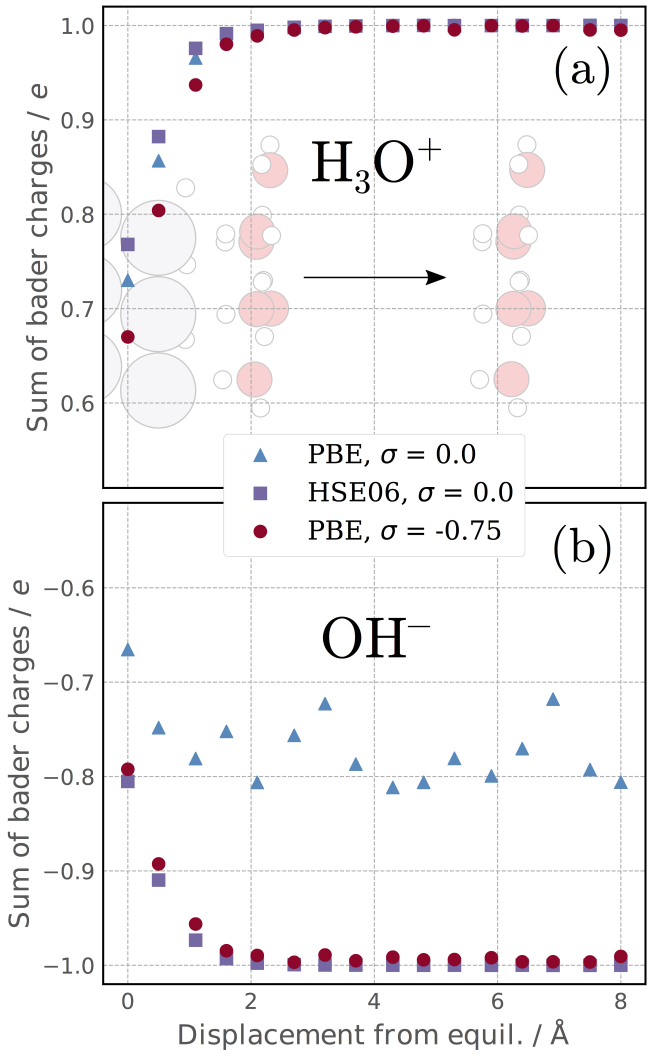

Fig. 3 Ionic charge, determined by summing the Bader charge of all electrolyte molecules, as a function of the distance from equilibrium near the metal surface, for (a) hydronium, and (b) hydroxide. For the GGA level with no added continuum charge (i.e. PBE, $\sigma = 0.0$), hydroxide exhibits clear SCT, with the ion charge being partial at all distances from the surface.

The ions are stabilized far from the surface with continuum solvation through VASPsol. To determine the charge on the ion at a given distance from equilibrium, the Bader charge partitioning scheme[39–41] is used to determine the charge on each atom in the simulation. Following the approach used previously,[23] the total ionic charge q_{ion} is given by

$$q_{\text{ion}} = \sum_{i}^{n_{\text{solv.}}} q_i. \tag{2}$$

Here $n_{\text{solv.}}$ is the number of atoms in the electrolyte, and q_i is the Bader charge on the given atom in the electrolyte. In other words, the ionic charge is taken to be the sum of all charges on atoms in the solvent bilayer. We show the above ionic charge q_{ion} for both hydronium and hydroxide as a function of its position relative to equilibrium in Figure 3, at both the GGA and hybrid level with varying amounts of the total number of electrons in the system. In all cases, implicit solvation was applied to ensure proper solvation of the electrolyte bilayer far from the surface.

Figure 3(a) shows the hydronium ionic charge as the solvent bilayer is moved away from the surface at both the GGA and hybrid levels. This analysis was carried out both with and without additional continuum charging. As we reported previously, the agreement between the GGA and hybrid level is quite good[23], with less than 0.05 e difference at all points. The addition of excess surface electron density on the surface changes the measured ionic charge near the surface. Excess surface charge changes the electron density decay behavior of the surface, thereby affecting the resulting ionic charge by about 0.06 e in the case of hydronium when 0.75 excess electrons are put into the simulation. The charge decreases by an additional 0.03 e when 1.0 excess electrons are put into the simulation.

Unlike the case of hydronium, the partial charge on hydroxide is not easily rationalized from a charge density overlap analysis, as we show in Supplementary Info Note 1. Furthermore, a direct comparison of the GGA and hybrid level is complicated by SCT with no excess surface charge, shown in Figure 3(b). As the hydroxide ion is moved away from the surface with $\sigma = 0.0$, the calculated ionic charge exhibits instability, fluctuating between 0.7 and 0.8e, largely due to SCT. When excess surface charge is introduced, pushing the system out of SCT, the measured ionic charge stabilizes and agrees quite well with the hybrid results. We note that, as seen in the case of hydronium, Figure 3 (a), the excess surface charge can affect the calculated ionic charge near the surface. Since this perturbation resulted in less than 0.1e change in ionic charge in the case of hydronium, we conclude that the hybrid and GGA levels agree in the case of hydroxide.

The partial ion charge has implications for the potential dependence of reactions involving the ion; for example, coupled proton-electron transfer reactions which can utilize both hydronium and hydroxide as a donor. As we outlined in recent works,[44,45] the potential dependence of a chemical reaction (i.e. its effective charge) is given by the slope of the reaction energy as a function of the work function averaged between the initial and final states. In the case of the Volmer reaction in acid (i.e. $(\mathrm{H}^+ + \mathrm{e}^-) + * \rightarrow \mathrm{H}*$), this slope is approximately 0.7[24,45–49], cor-

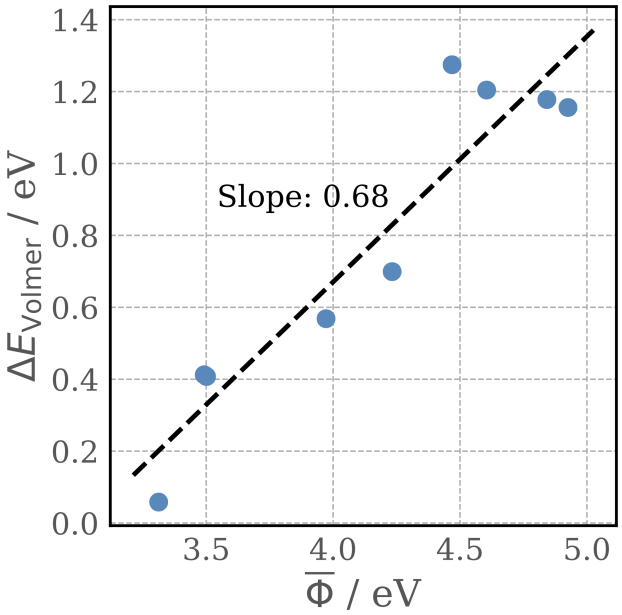

Fig. 4 Alkaline Volmer reaction energy, i.e. $H_2O+e^-+*\rightarrow H*+OH^-$, as a function of potential showing a slope of 0.7. This potential dependence is the same as that observed in the acidic Volmer reaction, i.e. $(H^+ + e^-) + * \rightarrow H*$.

responding to the partial charge of the ion near the surface.[23] Shown in Figure 4 is the Volmer reaction energy in base (i.e. $H_2O+e^-+*\rightarrow H*+OH^-$), showing a potential dependence of approximately 0.7. In other words, changing the potential of the electrode by 1 V only changes the reaction energy by 0.7 eV. The remaining potential dependence must then be accounted for by the reaction process (in the case of acidic Volmer) bringing a proton from the bulk to a position close to the surface, or (in the case of alkaline Volmer) moving the hydroxide from the surface to the bulk. An illustration of the referencing of electrochemical reaction barriers is given in the SI, as Figure S4 found in Note 4.

4 Conclusions

To summarize, we have shown here that due to the well-known failure of DFT to accurately describe band levels, the treatment of ions at the interface with GGA level DFT can be technically challenging, especially in the case of anions. However, these issues can be mitigated by introducing excess surface charge, with countercharge placed by (for instance) solving the linearized Poisson-Boltzmann equation as implemented in the VASPsol. We then show that hydroxide ions in the outer Helmholtz plane have a fractional charge of -0.8 to -0.7 e at both the GGA and hybrid levels of DFT. Although this fractional charge cannot easily be explained by a simple spillover analysis as in the case of hydronium, we show that the fractional charge is not a result of the DFT delocalization error, since both the GGA and hybrid levels predict a charge of unity as the ion moves away from the interface. While hybrid functionals such as HSE06 do not completely eliminate the well known DFT self-interaction error, they represent a good benchmark for extended metal systems where higher level methods are not practical. Benchmarking to wavefunction methods through, for example, many body perturbation theory[50,51] via Green's function techniques would be a useful future study. This work has implications for electrochemical kinetics involving reactions in basic media, since the calculation of electrochemical barriers typically involves either the initial or final state with an ion in the outer Helmholtz plane. Whereas many previous works using the computational hydrogen electrode (CHE)[52] assume an equilibrium between the ion in the Helmholtz plane and the ion in bulk, we emphasize that the computed transition states in such simulations should be referenced to bulk ions in order to obtain an accurate ion-electron transfer barrier. A full metadynamics trajectory studying the transfer of a proton (or hydroxide) from the bulk to the Helmholtz plane would be an interesting future study, as this would provide details on the kinetic barriers associated with the process.[53,54]

Conflicts of interest

There are no conflicts to declare.

Acknowledgements

This work was performed under the Joint Center for Artificial Photosynthesis, a DOE Energy Innovation Hub, supported through the Office of Science of the U.S. Department of Energy under Award Number DE-SC0004993. This work uses computational resources at the the Stanford Research Computing Center and also of the National Energy Research Scientific Computing Center, a DOE Office of Science User Facility, supported by the Office of Science of the U.S. Department of Energy under Contract No. DE-AC02-05CH11231. Some of the computing for this project was performed on the Sherlock cluster. KC acknowledges support by a research grant (9455) from VILLUM FONDEN.

Notes and references

1 Z. W. Seh, J. Kibsgaard, C. F. Dickens, I. Chorkendorff, J. K. Nørskov and T. F. Jaramillo, *Science*, 2017, **355**, year.

2 *Lazard's Levelized Cost of Energy Analysis - Version 12.0*, 2018, `https://www.lazard.com/media/450784/lazards-levelized-cost-of-energy-version-120-vfinal.pdf`.

3 P. De Luna, C. Hahn, D. Higgins, S. A. Jaffer, T. F. Jaramillo and E. H. Sargent, *Science*, 2019, **364**, eaav3506.

4 M. Jouny, W. Luc and F. Jiao, *Industrial & Engineering Chemistry Research*, 2018, **57**, 2165–2177.

5 A. R. Singh, B. A. Rohr, J. A. Schwalbe, M. Cargnello, K. Chan, T. F. Jaramillo, I. Chorkendorff and J. K. Nørskov, 2016.

6 J. M. McEnaney, A. R. Singh, J. A. Schwalbe, J. Kibsgaard, J. C. Lin, M. Cargnello, T. F. Jaramillo and J. K. Nørskov, *Energy & Environmental Science*, 2017, **10**, 1621–1630.

7 L. Wang, M. Xia, H. Wang, K. Huang, C. Qian, C. T. Maravelias and G. A. Ozin, *Joule*, 2018, **2**, 1055–1074.

8 S. Nitopi, E. Bertheussen, S. B. Scott, X. Liu, A. K. Engstfeld, S. Horch, B. Seger, I. E. Stephens, K. Chan, C. Hahn *et al.*, *Chemical reviews*, 2019.

9 F. Creazzo, D. R. Galimberti, S. Pezzotti and M.-P. Gaigeot, *The Journal of chemical physics*, 2019, **150**, 041721.

10 J. Klimeš, D. R. Bowler and A. Michaelides, *Journal of Physics: Condensed Matter*, 2009, **22**, 022201.

11 J. Carrasco, A. Hodgson and A. Michaelides, *Nature materials*, 2012, **11**, 667.

12 C. M. Gray, K. Saravanan, G. Wang and J. A. Keith, *Molecular Simulation*, 2017, **43**, 420–427.

13 J. Wellendorff, K. T. Lundgaard, A. Møgelhøj, V. Petzold, D. D. Landis, J. K. Nørskov, T. Bligaard and K. W. Jacobsen, *Physical Review B*, 2012, **85**, 235149.

14 F. Tran, J. Stelzl and P. Blaha, *The Journal of chemical physics*, 2016, **144**, 204120.

15 J. P. Perdew and K. Schmidt, *AIP Conference Proceedings*, 2001, **577**, 1–20.

16 A. J. Cohen, P. Mori-Sánchez and W. Yang, *Science*, 2008, **321**, 792–794.

17 M. Lundberg and P. E. Siegbahn, *The Journal of chemical physics*, 2005, **122**, 224103.

18 P. Mori-Sánchez, A. J. Cohen and W. Yang, *Physical review letters*, 2008, **100**, 146401.

19 C. Li, X. Zheng, A. J. Cohen, P. Mori-Sánchez and W. Yang, *Physical review letters*, 2015, **114**, 053001.

20 A. J. Cohen, P. Mori-Sánchez and W. Yang, *Chemical reviews*, 2011, **112**, 289–320.

21 J. P. Perdew, *International Journal of Quantum Chemistry*, 1985, **28**, 497–523.

22 M. E. Björketun, Z. Zeng, R. Ahmed, V. Tripkovic, K. S. Thygesen and J. Rossmeisl, *Chemical Physics Letters*, 2013, **555**, 145–148.

23 L. D. Chen, M. Bajdich, J. M. P. Martirez, C. M. Krauter, J. A. Gauthier, E. A. Carter, A. C. Luntz, K. Chan and J. K. Nørskov, *Nature Communications*, 2018, **9**, 3202.

24 P. Lindgren, G. Kastlunger and A. A. Peterson, *ACS Catalysis*, 2020, **10**, 121–128.

25 F. Nattino, C. Dupont, N. Marzari and O. Andreussi, *arXiv preprint arXiv:1906.00822*, 2019.

26 G. Kresse and J. Hafner, *Physical Review B*, 1993, **47**, 558–561.

27 G. Kresse and J. Furthmüller, *Physical Review B*, 1996, **54**, 11169–11186.

28 G. Kresse and J. Furthmüller, *Computational Materials Science*, 1996, **6**, 15–50.

29 K. Mathew and R. G. Hennig, *arXiv preprint arXiv:1601.03346*, 2016.

30 K. Mathew, R. Sundararaman, K. Letchworth-Weaver, T. Arias and R. G. Hennig, *The Journal of Chemical Physics*, 2014, **140**, 084106.

31 G. Kresse, *Physical Review B*, 1999, **59**, 1758–1775.

32 J. P. Perdew, K. Burke and M. Ernzerhof, *Physical Review Letters*, 1996, **77**, 3865–3868.

33 A. V. Krukau, O. A. Vydrov, A. F. Izmaylov and G. E. Scuseria, *The Journal of chemical physics*, 2006, **125**, 224106.

34 H. J. Monkhorst and J. D. Pack, *Physical Review B*, 1976, **13**, 5188.

35 W. P. Davey, *Physical Review*, 1925, **25**, 753.

36 K. T. Winther, M. J. Hoffmann, J. R. Boes, O. Mamun, M. Bajdich and T. Bligaard, *Scientific data*, 2019, **6**, 75.

37 J. A. Gauthier, L. D. Chen, M. Bajdich and K. Chan, `https://www.catalysis-hub.org/publications/GauthierImplications2019`.

38 J. A. Gauthier, S. Ringe, C. F. Dickens, A. J. Garza, A. T. Bell, M. Head-Gordon, J. K. Nørskov and K. Chan, *ACS Catalysis*, 2018, **9**, 920–931.

39 W. Tang, E. Sanville and G. Henkelman, *Journal of Physics: Condensed Matter*, 2009, **21**, 084204.

40 E. Sanville, S. D. Kenny, R. Smith and G. Henkelman, *Journal of Computational Chemistry*, 2007, **28**, 899–908.

41 G. Henkelman, A. Arnaldsson and H. Jónsson, *Computational Materials Science*, 2006, **36**, 354–360.

42 J. Heyd, G. E. Scuseria and M. Ernzerhof, *The Journal of chemical physics*, 2003, **118**, 8207–8215.

43 F. Liu and H. J. Kulik, *Journal of chemical theory and computation*, 2019.

44 J. A. Gauthier, C. F. Dickens, S. Ringe and K. Chan, *ChemPhysChem*, 2019.

45 J. A. Gauthier, C. F. Dickens, H. H. Heenen, V. Sudarshan, S. Ringe and K. Chan, *Journal of chemical theory and computation*, 2019.

46 K. Chan and J. K. Nørskov, *The Journal of Physical Chemistry Letters*, 2016, **7**, 1686–1690.

47 K. Chan and J. K. Nørskov, *The Journal of Physical Chemistry Letters*, 2015, **6**, 2663–2668.

48 S. Sakong and A. Groß, *The Journal of Chemical Physics*, 2018, **149**, 084705.

49 X. Liu, J. Xiao, H. Peng, X. Hong, K. Chan and J. K. Nørskov, *Nature Communications*, 2017, **8**, 15438.

50 R. J. Bartlett, *Annual Review of Physical Chemistry*, 1981, **32**, 359–401.

51 A. Tichai, J. Langhammer, S. Binder and R. Roth, *Physics Letters B*, 2016, **756**, 283–288.

52 J. K. Nørskov, J. Rossmeisl, A. Logadottir, L. Lindqvist, J. R. Kitchin, T. Bligaard and H. Jonsson, *The Journal of Physical Chemistry B*, 2004, **108**, 17886–17892.

53 J. Behler, R. Martoňák, D. Donadio and M. Parrinello, *Physical Review Letters*, 2008, **100**, 185501.

54 A. Barducci, M. Bonomi and M. Parrinello, *Wiley Interdisciplinary Reviews: Computational Molecular Science*, 2011, **1**, 826–843.